

Magnetic field-induced twin boundary motion in polycrystalline Ni–Mn–Ga fibres

To cite this article: N Scheerbaum *et al* 2008 *New J. Phys.* **10** 073002

View the [article online](#) for updates and enhancements.

Related content

- [Magnetically induced reorientation of martensite variants in constrained epitaxial Ni–Mn–Ga films grown on MgO\(001\)](#)
M Thomas, O Heczko, J Buschbeck *et al.*
- [Effects of film thickness and composition on the structure and martensitic transition of epitaxial off-stoichiometric Ni–Mn–Ga magnetic shape memory films](#)
Yuansu Luo, Philipp Leicht, Aleksej Laptev *et al.*
- [Microstructure and atomic configuration of the \(001\)-oriented surface of epitaxial Ni–Mn–Ga thin films](#)
P Leicht, A Laptev, M Fonin *et al.*

Recent citations

- [Amorphous microwires of high entropy alloys with large magnetocaloric effect](#)
Wei Sheng *et al*
- [Compressive deformation of polycrystalline Ni–Mn–Ga alloys near chemical ordering transition temperature](#)
L.S. Wei *et al*
- [Ni–Mn–Ga micro-trusses via sintering of 3D-printed inks containing elemental powders](#)
Shannon L. Taylor *et al*

Magnetic field-induced twin boundary motion in polycrystalline Ni–Mn–Ga fibres

N Scheerbaum¹, O Heczko, J Liu, D Hinz, L Schultz and O Gutfleisch

IFW Dresden, Institute for Metallic Materials, PO Box 270116,
D-01171 Dresden, Germany
E-mail: n.scheerbaum@ifw-dresden.de

New Journal of Physics **10** (2008) 073002 (8pp)

Received 11 April 2008

Published 1 July 2008

Online at <http://www.njp.org/>

doi:10.1088/1367-2630/10/7/073002

Abstract. Magnetic field-induced twin boundary motion leading to large magnetic field-induced strain of $\sim 1.0\%$ was established in polycrystalline Ni_{50.9}Mn_{27.1}Ga_{22.0} (at.%) fibres at room temperature (~ 60 – $100\ \mu\text{m}$ in diameter and $\sim 3\ \text{mm}$ in length). The fibres' grains are as large as the fibre diameter and of random orientation. At room temperature, a ferromagnetic 5M martensite is found. Magnetic field-induced twin boundary motion was indicated by magnetic measurements and validated by electron backscatter diffraction (EBSD). The application of a magnetic field shifts the equilibrium temperature of martensite and austenite by $\sim 0.4\ \text{K T}^{-1}$, which agrees with calculations using the Clapeyron–Clausius approach.

Contents

1. Introduction	2
2. Experimental	2
3. Results and discussion	3
4. Summary	7
Acknowledgment	8
References	8

¹ Author to whom any correspondence should be addressed.

1. Introduction

The capability of magnetic shape memory (MSM) alloys to produce large magnetic field-induced strain of several per cent has recently excited significant research interest [1]–[3]. In MSM alloys, the large strain can either be caused by a magnetic field-induced grain boundary (usually twin boundary) motion or by a magnetic field-induced phase transformation. The former is mostly referred to as MSM effect, magnetoplasticity [4, 5] or more precisely as magnetically induced reorientation (MIR) [6]. The magnetic field-induced phase transformation is correctly referred to as the MSM effect or as magnetically induced martensite/austenite (MIM/MIA). During MIR, twin boundaries move in order to allow those twin variants having a smaller angle between easy magnetization axis and applied field direction to grow, at the expense of unfavourably oriented twin variants [1, 7].

The most investigated MSM material so far is the Heusler alloy Ni_2MnGa , but also other MSM alloys and MSM–polymer-composites have been under scrutiny in order to overcome some of the disadvantages of (bulk) Ni_2MnGa , e.g. brittleness, difficult preparation and cost [8]–[13]. In Ni–Mn–Ga alloys near the stoichiometric composition Ni_2MnGa , MIR has been found in single crystals (resulting in up to $\sim 10\%$ strain) [3], in polycrystalline foams (resulting in 0.115% strain) [5], in polycrystalline melt-spun ribbons (resulting in 0.025% strain) [14] and in thin films (no macroscopic strain, as film was constrained) [6].

In this work, large MIR strain of $\sim 1.0\%$ in polycrystalline Ni_2MnGa fibres is reported. These fibres could be ideal for magnetically controlled MSM–polymer-composites. Textured MSM–polymer-composites are relatively simple to prepare in near-net-shape form by mixing MSM particles with a polymer and curing the polymer within a desired mould with an applied magnetic field [11, 12]. In these composites, stress-induced twin boundary motion has very recently been demonstrated by synchrotron x-ray and neutron diffraction [15, 16], making them promising for magnetically controlled mechanical energy dampers. On the other hand, a large magnetically induced strain (e.g. by MIR) within the MSM particles, as reported here, can result in MSM–polymer-composites being applied as actuators. A further advantage is the reduction of eddy currents for high actuation frequencies due to the nonconductive polymer matrix.

2. Experimental

$\text{Ni}_{50.9}\text{Mn}_{27.1}\text{Ga}_{22.0}$ (at.%, determined by inductively coupled plasma optical emission spectroscopy) fibres were prepared by crucible melt extraction. Their size is about 60–100 μm in diameter and several millimetres in length and they are polycrystalline. The fibres were annealed at 1100 $^\circ\text{C}$ for 2 h for homogenization and to stimulate grain growth. Their martensite–austenite transformation and Curie temperatures are well above room temperature ($M_s = 320\text{ K}$, $A_s = 328\text{ K}$ and $T_C = 371\text{ K}$). The martensite at room temperature has a pseudo tetragonal crystal structure with the modulation type 5M and uniaxial magnetocrystalline anisotropy. The fibres' actual crystallographic unit cell is slightly monoclinic, which was also found in a detailed XRD study of $\text{Ni}_{48.75}\text{Mn}_{29.75}\text{Ga}_{21.5}$ powder by Righi *et al* [17]. More information on the properties of the fibres can be found in [12]. Grain, (twin) boundary and texture information were obtained by scanning electron microscopy (SEM) and electron backscatter diffraction (EBSD) (LEO 1530 FEG-SEM equipped with a HKL Channel 5 EBSD unit). The unit cell used for the EBSD analysis was $a' = b' = a/\sqrt{2} = 4.20\text{ \AA}$, $c' = c = 5.58\text{ \AA}$ and space group $I4/mmm$ (139) (see figure 1(c)) [18]. In the EBSD maps, black lines are drawn between any two pixels, whenever

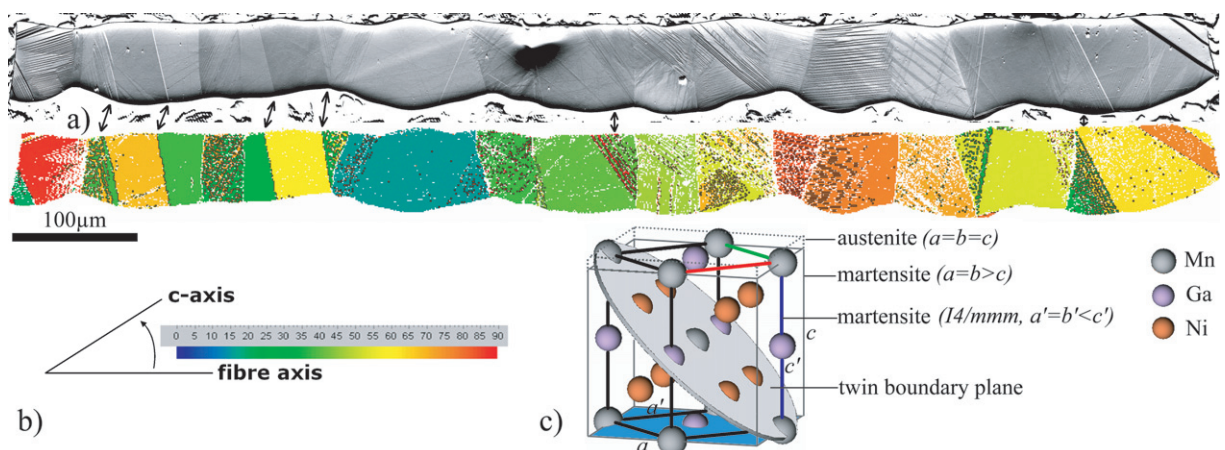


Figure 1. (a) SEM image using backscattered electron contrast (top) and EBSD mapping (bottom, step size $1\ \mu\text{m}$) of embedded Ni–Mn–Ga fibre. There are several twin boundaries present (black lines in EBSD map, some of them marked by arrows). (b) Colour code for all EBSD maps gives angular deviation between the crystallographic c -axis and the fibres' Z -direction (0° – 90° : blue–red). (c) Austenite (cubic $a = b = c \sim 0.58\ \text{nm}$, $L2_1$ ordered, thin solid and dashed lines) and both martensite unit cells. The conventional unit cell of the tetragonal martensite with $a = b > c$ ($c/a \sim 0.94$, thin solid lines) is derived from the austenite's $L2_1$ cubic axis. The martensite unit cell used for EBSD ($I4/mmm$ with $a' = b' < c'$, thick lines) describes the symmetry. The a – b -plane and the easy magnetization axis c are coloured blue.

their misorientation is an 86° rotation around rotation axis $\langle 110 \rangle$, short $86^\circ \langle 110 \rangle$, (with a 2° error for angle and axis). This corresponds to a twin misorientation $86^\circ \langle 100 \rangle$ on twin planes, when the unit cell is described with austenite's $L2_1$ cubic coordinate system having $c < a = b$ (see figure 1(c)). The theoretical misorientation angle between twin variants is $2 \cdot \arctan(c/a) = 86.4^\circ$. EBSD measurements are shown for two fibres. One fibre (length $\sim 1\ \text{mm}$) was embedded in epoxy and polished to study the inside of the fibre. A second fibre (length $\sim 3.5\ \text{mm}$) was placed on a silicon wafer and fixed with silver paste on one end. In this case, the EBSD patterns were collected from the fibre's surface. All EBSD maps shown are as-measured, apart from a removal of 'wild spikes' (one orientation pixel is surrounded totally by different orientations) and from filling single empty pixels, when surrounded totally by one orientation. The magnetic properties of this fibre were measured by a vibrating sample magnetometer (VSM) within a physical property measurement system (PPMS, Quantum Design).

3. Results and discussion

Figure 1 shows the fibres' bamboo-like grain structure with grains as large as the fibre diameter. Within the individual grains several twin boundaries are present and are marked in the EBSD map by black lines. There is no preferred crystallographic orientation of the grains, with respect to grain shape and fibre axis. As the fibre is rigidly fixed within the epoxy resin, a large MIR cannot be expected as it would be accompanied by a large strain. However, a small MIR was

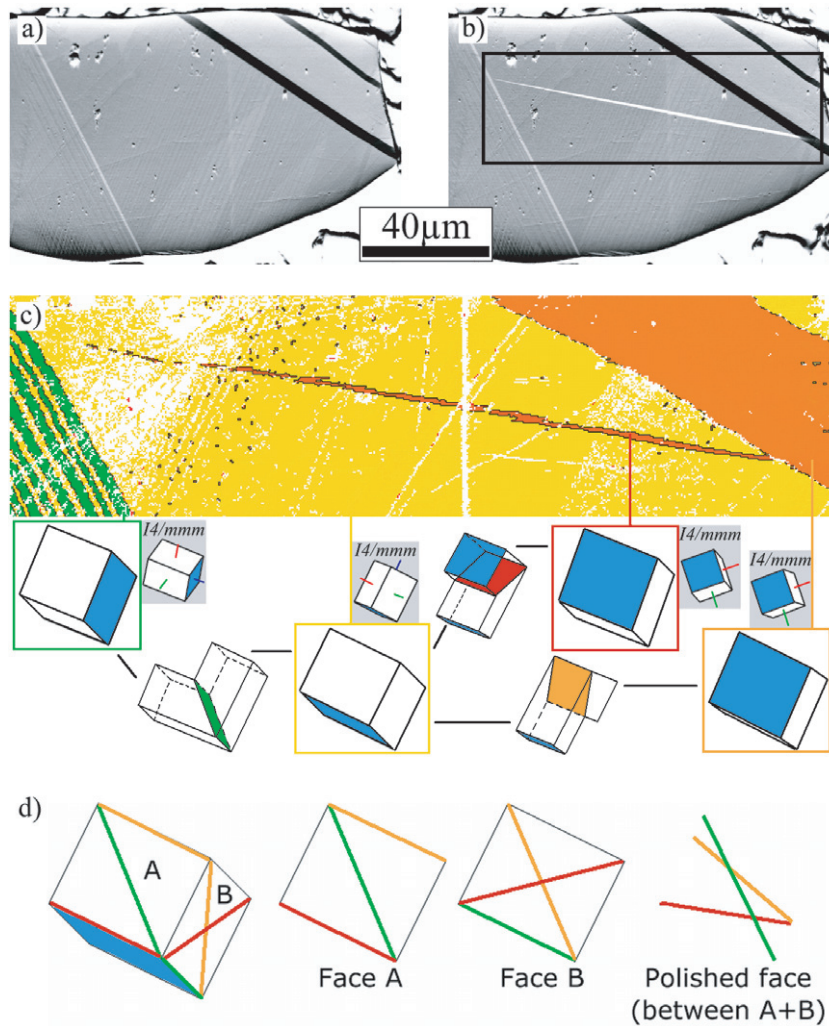


Figure 2. Embedded Ni–Mn–Ga fibre (from figure 1): (a) SEM image using backscattered electron contrast before and (b) after applying a magnetic field (~ 1.5 T). (c) EBSD map (step size $0.2 \mu\text{m}$) of marked area in (b). The crystallographic orientation is given with both unit cells, the $I4/mmm$ unit cell directly taken from the EBSD data (grey) and the corresponding unit cell using the cubic $L2_1$ -axis together with their twin boundaries (see figure 1(c)). (d) Explanation for observed angles between twin boundaries (green, orange and red). The polished face is cut between the faces A and B.

detected in one end of the fibre after applying a magnetic field (~ 1.5 T) several times parallel and perpendicular to the fibre axis (figure 2). A small twin lamella was formed having easy magnetization axis about perpendicular to the fibre axis. There are several different twin variants within the EBSD mapped area and their unit cell orientations as well as the corresponding twin boundaries are given in figure 2(c). As indicated by the black lines, the ‘yellow’ and ‘green’ variants are twin related (with ‘green’ twin boundary) by an 86.4° rotation with the rotation axis about perpendicular to the sheet plane. Likewise, the ‘yellow’ and ‘orange’ variants

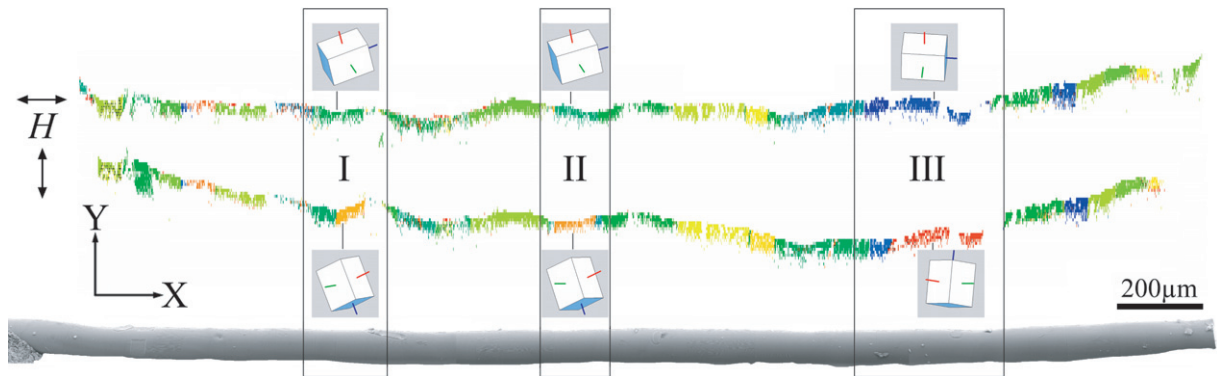


Figure 3. EBSD maps (step size $1 \mu\text{m}$) of the free Ni–Mn–Ga fibre after applying a magnetic field of $H = 2 \text{ T}$ parallel (top EBSD map) and perpendicular (lower EBSD map) to the fibre axis. The EBSD maps are vertically elongated (seven times) for better recognition. MIR is mainly found in the three regions I, II and III. The crystallographic orientation of these regions is indicated by the $I4/mmm$ unit cells (see figure 1(c)).

are twin related (with ‘orange’ twin boundary) by an 86.4° rotation around the rotation axis lying nearly within the sheet plane. The newly created, ‘red’ twin lamella has nearly the same orientation as the ‘orange’ twin variant (misorientation $\sim 7^\circ$). The rotation necessary to get from the ‘yellow’ to the ‘red’ twin variant is the same as to get from the ‘yellow’ to the ‘orange’ twin variant, except with an opposite sense of rotation (-86.4° , ‘red’ twin boundary), which explains the $\sim 7^\circ$ misorientation between the ‘red’ and ‘orange’ twin variants, $2(90^\circ - 86.4^\circ) = 7.2^\circ$. The observed angles between twin boundaries are due to their projection to the observation (polished) plane (figure 2(d)).

A large MIR strain of $\sim 1.0\%$ was found in a not constrained, polycrystalline and randomly textured fibre by magnetizing the fibre parallel and perpendicular to the fibre axis (by measuring $M(H)$ dependence up to 2 T). The fibre was only mounted on one end. The orientation distribution along the complete free length of the fibre was mapped by EBSD (figure 3) in order to determine those regions showing MIR. Three regions (grains) of the fibre were identified to show significant MIR, in each case over a length of $\sim 100\text{--}200 \mu\text{m}$ (table 1). The regions I–III yield a total MIR strain of $(24 \pm 2) \mu\text{m}$ along the fibre axis. The entire free part of the fibre ($\sim 2800 \mu\text{m}$) produces a MIR strain of $(29 \pm 2) \mu\text{m}$, which corresponds to $\sim 1.0\%$ strain. The additional strain most likely originates from several other smaller regions, which exhibit MIR and are not seen in the EBSD maps. The MIR strain was determined from EBSD maps (step size $1 \mu\text{m}$, therefore error is assumed as $\pm 2 \mu\text{m}$) and supported by SEM images.

The resulting strain ε in the X -direction (fibre axis) for a certain unit cell orientation can be estimated using the maximum theoretical strain along the crystallographic c -axis, $\varepsilon_0 = 1 - (a/c) = 6.1\%$, and the angle α between the crystallographic c -axis and the X -direction to $\varepsilon = \varepsilon_0 \cdot \cos(\alpha)$. The obtained values for each of the three regions, given in table 1, give an upper bound of $\sim 25 \mu\text{m}$ total strain to be expected along the fibre axis, which agrees well with the measured strain of $(24 \pm 2) \mu\text{m}$.

During magnetization of the fibre, typical MIR jumps were observed in the $M(H)$ curves shown in figure 4(a). These jumps represent a sudden volume increase of one crystallographic

Table 1. Parameters of the three regions exhibiting MIR in figure 3.

Region	Length in X -direction	Angle between (c and X)/(c and Y)		Strain in X -direction	
		Field in X (\parallel)	Field in Y (\perp)	Calculated	Measured
I	70–75 μm	23°/70°	70°/22°	5.6% \rightarrow 4 μm	4 μm
II	94 μm	19°/74°	72°/22°	5.8% \rightarrow 5 μm	4 μm
III	217–265 μm	5°/87°	85°/7°	6.1% \rightarrow 13–16 μm	16 μm
I + II + III	381–435 μm			22–25 μm	(24 \pm 2) μm
Entire fibre (free part)	\sim 2800 μm				(29 \pm 2) μm

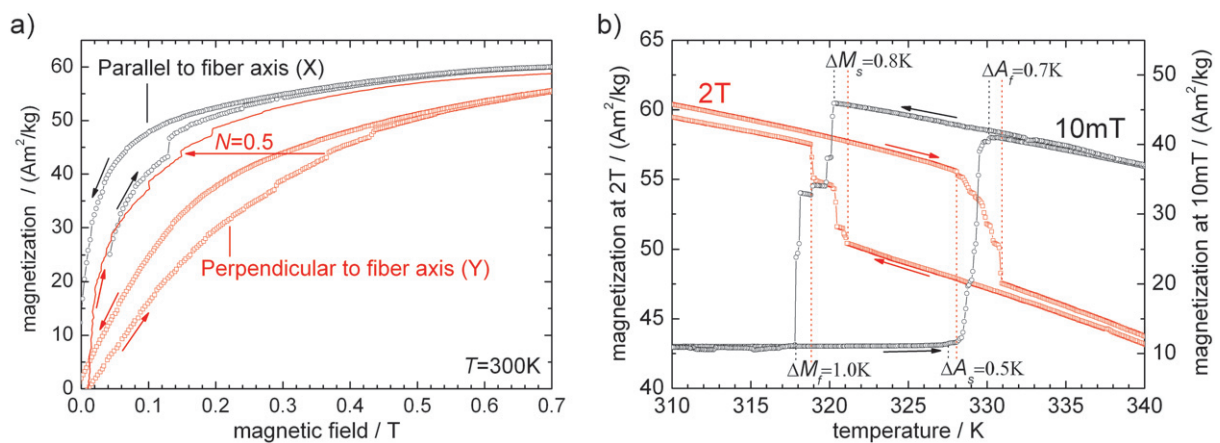


Figure 4. VSM measurement of the free Ni–Mn–Ga fibre: (a) $M(H)$ dependence parallel and perpendicular to the fibre axis taken before each corresponding EBSD map from figure 3. $M(H)$ curves were measured up to 2 T, only the low field part is shown for clarity. Additionally, $M(H)$ dependence in the Y -direction after a demagnetization correction using $N = 0.5$ is shown. (b) Stepwise martensite–austenite transformation and shift of transformation temperatures (heating/cooling rate 5 K min⁻¹).

orientation favourably oriented to the field direction, i.e. the growth of one twin variant by twin boundary motion [7, 19]. Since these jumps were only seen during the initial magnetization along one axis and were reversible by changing the applied field direction by 90°, they are a clear indication for MIR and are consistent with the EBSD results. The critical field (or switching field) for MIR parallel to the fibre axis is \sim 130 mT, which is particularly low, mainly due to the nearly zero demagnetization field in this fibre direction (aspect ratio of fibre $>$ 30). An even lower critical field needed for MIR was recently reported for an orthorhombic Ni₅₂Mn₂₃Ga₂₅ thin film and ascribed to the film's purity [6]. In the perpendicular direction, three MIR jumps are apparent, quite likely corresponding to the three MIR showing regions I–III observed in EBSD. A demagnetization correction for the perpendicular direction using $N = 0.5$ shows that the internal critical magnetic field for MIR is similar for the perpendicular and parallel directions.

Neither the constrained nor the free fibre showed MIR during the first magnetic field applications. The MIR shown here has been obtained after applying a field of 1.5–2 T several times (~ 5 times) in different directions. The application of a magnetic field in different directions generates an alternating force on the twin boundaries, which can increase the twin boundary mobility. For the free fibre, MIR has been achieved after an additional cooling from austenite to martensite in a saturation field of 2 T (in VSM) followed again by a magnetic field application in different directions (~ 4 times). As different twin boundaries may hinder each others movement, cooling to the martensite in a saturation magnetic field H favours the generation of one twin variant (with $c \parallel H$). Because of this, fewer twin boundaries are present, which can increase the twin boundary mobility. MIR was reversible and constant for at least ~ 5 cycles thereafter. It is likely that training the fibres with many more cycles can further increase the MIR exhibiting fraction of the fibre.

Although the preparation method of the fibres yields a rather homogeneous composition distribution, the martensite–austenite transformation of the free, single fibre shows a stepwise character in high resolution $M(T)$ measurements (figure 4(b)). These steps might be caused by different transformation temperatures of individual grains suggesting slight compositional differences between them.

Additionally, the $M(T)$ curve at 2 T (sample is saturated) is shifted to higher temperatures by slightly less than ~ 1 K compared to the $M(T)$ curve at 10 mT. In a saturation magnetic field H , the higher saturation magnetization M_{sat} of the martensite (compared to austenite) results in a lower Zeeman energy $-M_{\text{sat}} \cdot H$ of the martensite. This shifts the martensite–austenite transformation temperatures to higher temperatures. The (averaged) equilibrium temperature of martensite and austenite can be estimated by $T_{\text{m}} = (M_{\text{f}} + M_{\text{s}} + A_{\text{s}} + A_{\text{f}})/4$ [20], where M_{f} , M_{s} , A_{s} and A_{f} are the finish and start temperatures of the martensite–austenite transformation. With this, the measured temperature shift ΔT_{m} amounts to

$$T_{\text{m}}^{10\text{mT}} = (317.8 + 320.3 + 327.6 + 330.2)/4 = 323.96 \text{ K},$$

$$T_{\text{m}}^{2\text{T}} = (318.8 + 321.1 + 328.1 + 330.9)/4 = 324.73 \text{ K},$$

$$\Delta T_{\text{m}} = T_{\text{m}}^{2\text{T}} - T_{\text{m}}^{10\text{mT}} = 0.8 \text{ K}.$$

The theoretical temperature shift ΔT can be calculated by the Clapeyron–Clausius approach as $\Delta T = \mu_0 \cdot \Delta M_{\text{sat}} \cdot T_{\text{m}} \cdot H / Q$ [21] (anisotropy energy neglected), where $\Delta M_{\text{sat}} = (7.0 \pm 0.1) \text{ Am}^2 \text{ kg}^{-1}$ is the difference of saturation magnetization between the austenite and martensite, $\mu_0 H = 2 \text{ T}$ is the applied magnetic field, $T_{\text{m}} = T_{\text{m}}^{10\text{mT}} = 323.96 \text{ K}$ and $Q = (5.5 \pm 0.2) \times 10^3 \text{ J kg}^{-1}$ is the latent heat of the martensite–austenite transformation (determined from differential scanning calorimetry (DSC) measurements). The calculated shift $\Delta T = (0.82 \pm 0.05) \text{ K}$ agrees well with the measured value ΔT_{m} .

4. Summary

In summary, magnetic field-induced twin boundary motion (MIR) has been observed in melt-extracted polycrystalline $\text{Ni}_{50.9}\text{Mn}_{27.1}\text{Ga}_{22.0}$ (at.%) fibres, in both constrained and free states, resulting, in the case of the free fibre, in a large macroscopic strain of $\sim 1.0\%$. The fibres' grains

are as large as the fibre diameter and randomly oriented. As the fibres preferentially and easily break along grain boundaries, single crystalline MSM particles capable of MIR can be obtained. Thus, these fibres are an ideal precursor for the preparation of MSM–polymer-composites for magnetic field controlled actuators and dampers. A magnetic field of 2 T shifts the equilibrium temperature of the martensite and austenite by ~ 0.8 K, which agrees with calculations using the Clapeyron–Clausius approach.

Acknowledgment

This work is supported by DFG (SPP 1239) and Plansee SE (Reute, Austria).

References

- [1] Ullakko K, Huang J K, Kantner C, O’Handley R C and Kokorin V V 1996 *Appl. Phys. Lett.* **69** 1966–8
- [2] Vasil’ev A N, Buchel’nikov V D, Takagi T, Khovailo V V and Éstrin É 2003 *Phys.—Usp.* **46** 559–88
- [3] Sozinov A, Likhachev A A, Lanska N and Ullakko K 2002 *Appl. Phys. Lett.* **80** 1746–8
- [4] Kostorz G and Müllner P 2005 *Z. Metallk.* **96** 703–9
- [5] Boonyongmaneerat Y, Chmielus M, Dunand D C and Müllner P 2007 *Phys. Rev. Lett.* **99** 247201
- [6] Thomas M, Heczko O, Buschbeck J, Rößler U K, McCord J, Scheerbaum N, Schultz L and Fähler S 2008 *New J. Phys.* **10** 023040
- [7] Heczko O, Sozinov A and Ullakko K 2000 *IEEE Trans. Magn.* **36** 3266–8
- [8] James R D and Wuttig M 1998 *Phil. Mag. A* **77** 1273–99
- [9] Lavrov A N, Komiya S and Ando Y 2002 *Nature* **418** 385–6
- [10] Kainuma R *et al* 2006 *Nature* **439** 957–60
- [11] Feuchtwanger J, Michael S, Juang J, Bobo D, Goldie J and Berkowitz A 2003 *J. Appl. Phys.* **93** 8528–30
- [12] Scheerbaum N, Hinz D, Gutfleisch O, Müller K H and Schultz L 2007 *Acta Mater.* **55** 2707–13
- [13] Conti S, Lenz M and Rumpf M 2007 *J. Mech. Phys. Solids* **55** 1462–86
- [14] Guo S H, Zhang Y H, Quan B Y, Li J L and Wang X L 2005 *Mater. Sci. Forum* **475–479** 2009–12
- [15] Scheerbaum N, Hinz D, Gutfleisch O, Skrotzki W and Schultz L 2007 *J. Appl. Phys.* **101** 09C501
- [16] Feuchtwanger J, Lazpita P, Vidal N, Barandiaran J M, Gutierrez J, Hansen T, Peel M, Mondelli C, O’Handley R C and Allen S M 2008 *J. Phys.: Condens. Matter* **20** 104247
- [17] Righi L, Albertini F, Pareti L, Paoluzi A and Calestani G 2007 *Acta Mater.* **55** 5237–45
- [18] O’Handley R C, Murray S J, Marioni M, Nembach H and Allen S M 2000 *J. Appl. Phys.* **87** 4712–7
- [19] Heczko O 2005 *J. Magn. Magn. Mater.* **290** 787–94
- [20] Tong H C and Wayman C M 1974 *Acta Metall.* **22** 887–96
- [21] Vasil’ev A N, Bozhko A D, Khovailo V V, Dikshtein I E, Shavrov V G, Buchelnikov V D, Matsumoto M, Suzuki S, Takagi T and Tani J 1999 *Phys. Rev. B* **59** 1113–20